Inorganic Chemistry

Article

pubs.acs.org/IC

Crystallographic and Magnetic Phase Transitions in the Layered Ruthenium Oxyarsenides TbRuAsO and DyRuAsO

Michael A. McGuire,* Andrew F. May, and Brian C. Sales

Oak Ridge National Laboratory, Oak Ridge, Tennessee 37831, United States

Supporting Information

ABSTRACT: The crystallographic and physical properties of TbRuAsO and DyRuAsO at and below room temperature are reported, including full structure refinements from powder X-ray diffraction data and measured electrical and thermal transport properties, magnetic susceptibility, and heat capacity. Both compounds are isostructural to LaFeAsO (ZrCuSiAs-type, *P*4/*nmm*) at room temperature. However, DyRuAsO undergoes a symmetry-lowering crystallographic phase transition near 25 K, and adopts an orthorhombic structure (*Pmmn*) below this temperature. This structural distortion is unlike those observed in the analogous Fe compounds. Magnetic phase transitions are observed in both compounds which suggest antiferromagnetic ordering of lanthanide moments occurs near 7.0 K in TbRuAsO and 10.5 K in DyRuAsO. The nature of the structural distortion as well as thermal conductivity and heat capacity behaviors indicate strong coupling between the magnetism and the lattice. The behaviors of both materials show magnetic ordering of small moments on Ru may occur at low temperatures.

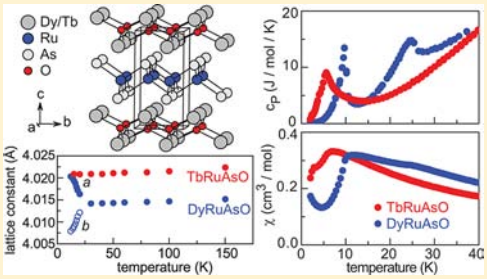

INTRODUCTION

Interest in superconductivity has motivated intense study of layered iron-pnictides and chalcogenides since the report of transition temperatures as high as 26 K in fluorine-doped LaFeAsO in 2008.[1] Subsequent research demonstrated not only superconductivity in many structurally related families of materials, but also interesting crystallographic and magnetic properties and phase transitions (for reviews, see refs 2−6). Superconductivity is intimately linked to magnetism in these compounds, and strong coupling between the crystal structure and the magnetism is present as well. Thus, studies of crystal structures and their relationships to physical properties are key in developing a better understanding of these interesting and potentially technologically useful materials.

Crystallographic information is particularly important for Fe-based superconductors and related compounds because, in many cases, structural phase transitions are associated with ordering of iron magnetic moments in nonsuperconducting (and some superconducting) compositions. These include ZrCuSiAs-type *Ln*FeAsO (*Ln* = La−Tb) and *Ae*FeAsF (*Ae* = Ca, Sr), $ThCr_2Si_2$-type $AeFe_2As_2$ (*Ae* = Ca, Sr, Ba), PbO- or Cu2Sb-type $Fe_{1+x}Q$ (*Q* = S, Se, Te), and the $ThCr_2Si_2$ derivatives $A_{1-y}Fe_{1-x}Q_2$ (*A* = K, Rb, Cs, Tl; *Q* = S, Se, Te). All of these materials are tetragonal at high temperature, and the Fe atoms form a square net in the *ab*-plane. The Fe net is capped above and below by pnictogens or chalcogens, giving edge-sharing tetrahedral coordination to the Fe sites. The crystallographic phase transitions distort the chemical environment around the Fe atoms in various ways. In *Ln*FeAsO and *Ae*FeAsF, the symmetry is lowered from *P*4/*nmm* to *Cmme* upon cooling.[7−12] The resulting distortion can be visualized as a stretching of the square net of Fe into a rectangular net. A similar distortion occurs in $AeFe_2As_2$ which transforms from space group *I*4/*mmm* to *Fmmm*.[13,14] Temperature, pressure, or chemical doping can induce a second type of crystallographic transition in these materials as well, resulting in a collapsed-tetragonal state with a reduced *c* lattice constant but retaining the parent tetragonal symmetry.[15] Three types of structural transitions occur in $Fe_{1+x}Q$. For *Q* = Se, the distortion is to an orthorhombic structure (*Cmme*) with a rectangular Fe net as in *Ln*FeAsO and $AeFe_2As_2$.[16] For *Q* = Te and a small amount of interstitial iron ($x \sim 0.08$) the low temperature structure is monoclinic ($P2_1/m$), while an orthorhombic (*Pmmn*) structure is observed at low temperature for larger values of *x*.[17,18] The orthorhombic distortion in $Fe_{1+x}Te$ is different from that previously described for the arsenide materials. In this case the Fe net is stretched across the diagonal of the Fe squares. The ternary chalcogenides $A_{1-y}Fe_{1-x}Q_2$ have disordered *A* and Fe vacancies at high temperatures (>400 K). At lower temperatures the Fe vacancies are ordered at least to some degree resulting in complex superstructures containing square plaquettes of Fe.[19−22] It is interesting to note that many similar crystallographic distortions can be induced in rare-earth copper pnictides by chemical substitution.[23,24]

Importantly, each of the temperature induced crystallographic distortions described above is accompanied by an Fe magnetic ordering transition. A particulary clear example of the interplay between structure, magnetism, and superconductivity can be found in $Ba(Fe_{1-x}Co_x)_2As_2$. For certain compositions,

Received: May 22, 2012
Published: July 26, 2012

dx.doi.org/10.1021/ic3010695 | *Inorg. Chem.* 2012, 51, 8502−8508

upon cooling, these materials experience a structural distortion and antiferromagnetic ordering transition followed by a superconducting transition at lower temperatures. At the superconducting transition, the ordered magnetic moment decreases as does the magnitude of the orthrhombic distortion, showing a strong link among the superconductivity, magnetism, and crystal structure.[25,26]

Clearly, crystallographic phase transitions are quite common in these types of layered Fe compounds. However, they also occur in analogous materials with other transition metals. There are relatively few examples of this, but this may be in part because of the increased attention paid to the Fe materials to date. Examples with other transition metals include $BaNi_2As_2$, which transforms to a triclinic structure at low temperature,[27] and $SrRh_2As_2$ which adopts three polymorphs, including the $ThCr_2Si_2$ structure at high temperatures.[28]

Iron is formally divalent (or nearly so) in each of the Fe-based superconductor families. However, as is often the case in these types of material, formal charges are not sufficient for understanding the physical behaviors. For example, substitution of Fe with isoelectronic Ru produces some perhaps unexpected behaviors: superconductivity can be induced by Ru-doping $AeFe_2As_2$.[29,30] Interestingly, superconductivity has not been observed in Ru-doped *Ln*FeAsO.[31,32] Although Ru and Fe are formally isovalent, the larger size of Ru and more extended nature of its 4d electrons results in significant differences in crystal structure as well as magnetic and electronic properties. These effects, as well as chemical disorder, are important in determining the behavior of Ru-doped systems.[31−33]

We have recently investigated the effects of full substitution of Ru for Fe in ZrCuSiAs-type oxyarsenides. *Ln*RuAsO for *Ln* = Ce, Nd, Sm, and Gd appear to be normal metals with no indication of Ru magnetism or structural distortions at low temperature.[34] In the present work we have extended our investigation of the structure and physical properties of *Ln*RuAsO to *Ln* = Tb and Dy, the heaviest lanthanides for which the structure is known to be stable.[7] Both of these compounds were found to have low temperature phase transitions indicating long-range antiferromagnetic ordering of rare-earth magnetic moments occurring near 7.0 K in TbRuAsO and 10.5 K in DyRuAsO. In addition, a crystallographic phase transition occurs near 25 K in DyRuAsO, from the high temperature tetragonal to a low temperature orthorhombic (*Pmmn*) structure. This is the first example of a structural phase transition in a ZrCuSiAs-type oxypnictide without Fe, and the first example of a transition from *P*4/*nmm* to *Pmmn* in the iron-pnictide families. Physical properties measurements reveal strong coupling between the crystallographic and magnetic phase transitions. This is reminiscent of the magneto-elastic coupling in the Fe compounds; however, here magnetism of the lanthanide may be more important than that of the transition metal. This work highlights the important role that the lanthanide element can play in determining the crystallographic, electronic, and magnetic behavior of ZrCuSiAs-type oxypnictides.

RESULTS AND DISCUSSION

Crystal Structure. Powder diffraction results for TbRuAsO and DyRuAsO at room temperature are presented in Figure 1a and 1b, respectively, and refinement results are summarized in Table 1. The samples are about 90% pure, and contain RuAs and Dy_2O_3 or Tb_2O_3 as secondary phases. At this temperature, both materials adopt the tetragonal ZrCuSiAs structure-type

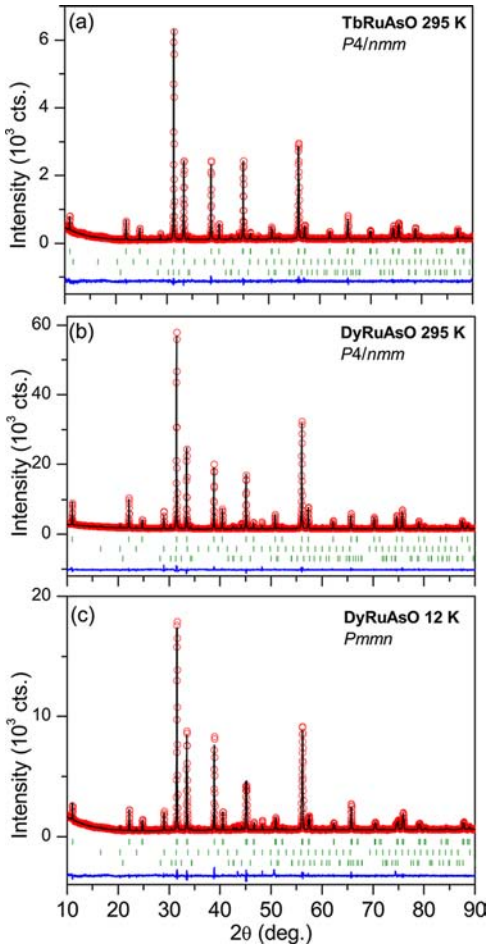

Figure 1. Results of Rietveld refinement of powder X-ray diffraction data for (a) TbRuAsO at 295 K, (b) DyRuAsO at 295 K, and (c) DyRuAsO at 12 K. The measured data are shown as circles and the fitted profile as a line through the data. The difference curves are shown as a line at the bottom of each panel. Tick marks locate Bragg reflections from the main phase (upper set of tics), rare-earth sesquioxide (middle set), and RuAs (lower set).

(Figure 2a). This is the same crystal structure adopted by LaFeAsO and many quaternary rare-earth transition metal oxypnictides.[7,35,36] Lattice constants and interatomic distances and angles continue the trends observed for the La, Nd, Sm, and Gd compounds,[34] and the lattice constants agree well with the literature values.[7] The tetrahedral coordination around Ru continues to become more regular as the size of the lanthanide is reduced, but is still quite distorted for TbRuAsO and DyRuAsO. This is indicated by the angle α (Figure 2a), which is 112.57(5)° for TbRuAsO and 112.38(2)° for DyRuAsO. These should be compared to the value for ideal tetrahedral coordination of 109.47°, and to the value determined for TbFeAsO of 109.57(1)°.[37] The coordination around the transition metal is significantly more distorted in the Ru materials than in the Fe compounds across the lanthanide series, perhaps because of direct Ru−Ru interactions.[34]

Diffraction patterns from TbRuAsO at temperatures down to 15 K were well described by the ZrCuSiAs structure-type. However, low temperature measurements indicated DyRuAsO undergoes a symmetry lowering crystallographic phase transition upon cooling. Powder diffraction results at 12 K for this material are shown in Figure 1c, and refinement results are given in Table 1. At low temperature, the symmetry of

dx.doi.org/10.1021/ic3010695 | Inorg. Chem. 2012, 51, 8502−8508

Table 1. Results of Rietveld Refinement of TbRuAsO and DyRuAsO from Powder X-ray Diffraction Data

	compound		
	TbRuAsO	DyRuAsO	DyRuAsO
temperature	295 K	295 K	12 K
space group	*P*4/*nmm*	*P*4/*nmm*	*Pmmn*
a (Å)	4.02540(9)	4.01728(3)	4.02033(7)
b (Å)			4.00791(7)
c (Å)	8.0710(2)	8.03272(7)	8.00483(15)
$z_{Tb/Dy}$	0.1334(2)	0.13157(9)	0.1318(2)
z_{Ru}	0.5	0.5	0.5007(6)
z_{As}	0.6664(3)	0.66747(15)	0.6682(3)
z_{O}	0	0	−0.009(4)
$B_{overall}$	0.33(4)	0.57(2)	0.41(3)
R_{Bragg}	3.8	3.8	3.3
R_p	6.88	2.86	4.82
R_wp	9.19	3.9	7.26
χ^2	1.54	3.12	3.92
$d_{Tb/Dy-O}$ (Å)	2.2825(7) ×4	2.2697(4) ×4	2.305(16) ×2
			2.232(14) ×2
$d_{Tb/Dy-As}$ (Å)	3.2731(14) ×4	3.2673(7) ×4	3.2587(14) ×4
d_{Ru-As} (Å)	2.4196(13) ×4	2.4175(7) ×4	2.416(3) ×2
			2.417(3) ×2

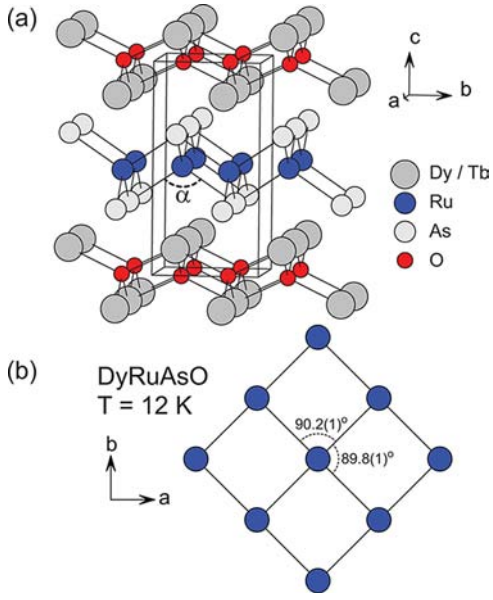

Figure 2. Representation of the crystal structure of TbRuAsO and DyRuAsO. In panel (a) the unit cell is outlined, and the angle α describing the Ru coordination environment is labeled. This structure is tetragonal for both materials at room temperature. For DyRuAsO at 12 K, the unit cell is orthorhombic ($a > b$). Panel (b) shows the Ru net in DyRuAsO at 12 K with the slightly distorted angles labeled.

DyRuAsO is lowered from space group *P*4/*nmm* to *Pmmn*, which corresponds a distortion in the *ab*-plane by expanding along the *a* direction and compressing along the *b* direction. As noted above, this is the same distortion that occurs upon cooling in iron-rich $Fe_{1+x}Te$,[17,18] but it is unlike the orthorhombic distortion to space group *Cmme* that is common in Fe-containing ZrCuSiAs-type materials. Since the square Ru net is rotated by 90° with respect to the unit cell axes, the low temperature structure has a single Ru−Ru distance, but a network with angles which deviate slightly from 90°. This is illustrated in Figure 2. The square nets of oxygen present at high temperature are distorted in this same way, while the Dy and As nets become rectangular at low temperatures.

To determine the structural phase transition temperature T_S, powder diffraction data were collected as a function of temperature. Figure 3 shows the temperature dependence of

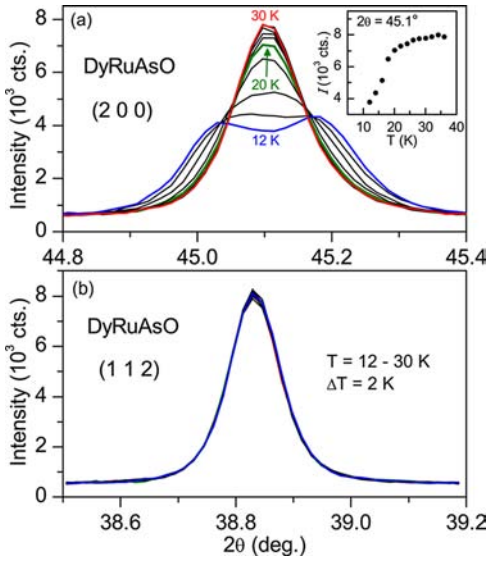

Figure 3. Temperature evolution of (a) the (2 0 0) and (b) the (1 1 2) Bragg reflections for DyRuAsO. Upon transforming from *P*4/*nmm* to *Pmmn*, the (2 0 0) reflection is split into (2 0 0) and (0 2 0), while the (1 1 2) reflection is not affected. The inset in (a) shows the temperature dependence of the diffracted intensity at 45.1°, which decreases as the distortion increases.

the (2 0 0) and (1 1 2) reflection from DyRuAsO between 12 and 30 K. The crystallographic distortion (*P*4/*nmm* to *Pmmn*) results in a broadening and eventual splitting of the (2 0 0) peak, while the (1 1 2) peak remains single and sharp, as expected for this distortion. For the *P*4/*nmm*−*Cmme* distortion that occurs in isostructural Fe compounds, the (1 1 2) reflection is split and the (2 0 0) reflection is not. The inset in Figure 3a shows the temperature dependence of the measured intensity at the center of the tetragonal (2 0 0) peak. These results show that a sharp change in structure occurs near 20 K, but that the distortion begins at higher temperatures, between 20 and 30 K.

The temperature dependence of the unit cell parameters for TbRuAsO and DyRuAsO are shown in Figure 4. Normal thermal expansion behavior is observed for TbRuAsO. For DyRuAsO at temperatures of 20 K and below, the orthorhombic model resulted in a lower value of χ^2 than the tetragonal model. At 30 K and higher, fitting with the orthorhombic model gave indistinguishable values of *a* and *b*, a higher value of χ^2 than *P*4/*nmm*, or was unstable. This shows that T_S lies between 20 and 30 K, consistent with the peak shapes shown in Figure 3.

Inspection of the atomic positions listed in Table 1 shows that the Ru and O layers are flat at room temperature, but a slight puckering is indicated in the low temperature phase of DyRuAsO by the deviation of the *z*-coordinate from 1/2 for Ru and 0 for O. Similar puckering is indicated in the related rare-earth copper pnictides.[23,24] The consequences of this on the interatomic distances are small. Upon distortion from the tetragonal to orthorhombic structure, the bond distances are

dx.doi.org/10.1021/ic3010695 | *Inorg. Chem.* 2012, 51, 8502−8508

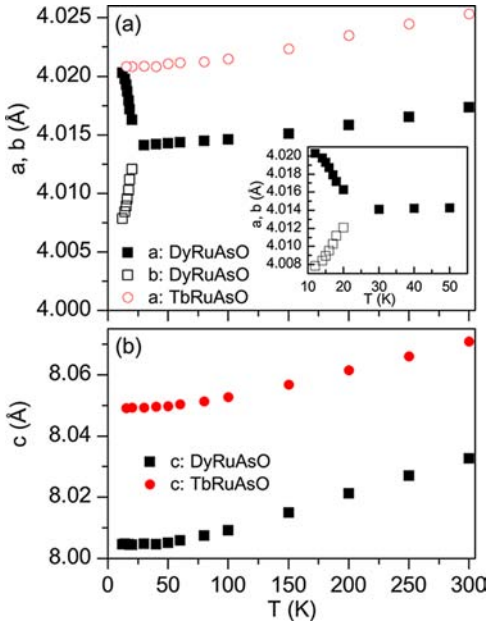

Figure 4. Temperature dependence of the lattice constants of TbRuAsO (circles) and DyRuAsO (squares) determined from Rietveld refinement. For DyRuAsO, *a* and *b* diverge below 30 K as the symmetry is lowered from tetragonal to orthorhombic.

primarily affected by the lattice constant changes. Effects on selected interatomic distances are summarized in Table 1. The most significant distortion occurs around Dy, and in particular in the Dy−O bonding. At room temperature, there is a single Dy−O distance of 2.2697(4)Å. At 12 K there are two inequivalent Dy−O distances of 2.232(14) and 2.305(16) Å which differ by 0.07 Å. It may be expected that such a change in coordination would have consequences on the crystalline electric field at the Dy site and therefore affect the magnetic properties of this material, which should be dominated by the Dy magnetic moment. Discussion of the physical properties below will show that indeed significant magneto-elastic interactions are present in DyRuAsO.

Magnetization, Heat Capacity, and Transport Properties. The low temperature magnetic behavior of TbRuAsO and DyRuAsO are summarized in Figures 5 and 6. A sharp decrease is observed in the low field direct current (DC) magnetization (Figure 5) and real part of the alternating current (AC) susceptibility (Figure 6). This indicates antiferromagnetic ordering occurs at T_N = 7.0 K for TbRuAsO and T_N = 10.5 K for DyRuAsO. At higher fields, these features are suppressed, and the field dependence of the magnetization is nonlinear at the lowest temperatures, as seen in the insets of Figure 5. Reorientation of the lanthanide magnetic moments induced by external field is likely responsible for this behavior.

The measured DC susceptibility was fit using the Curie−Weiss model over the temperature range of 75−300 K. The fitted Curie constants indicate effective moments per formula unit of 9.6 μ_B for TbRuAsO and 10.9 μ_B for DyRuAsO, in good agreement with the expected trivalent, lanthanide, free-ion values of 9.7 and 10.7 μ_B, respectively. Weiss temperatures were negative, consistent with antiferromagnetic interactions, with values of −24 K for TbRuAsO and −17 K for DyRuAsO.

Additional anomalies are observed for DyRuAsO near 25 K in the low field DC magnetization (Figure 5) and the AC susceptibility (Figure 6). This is identified as the structural

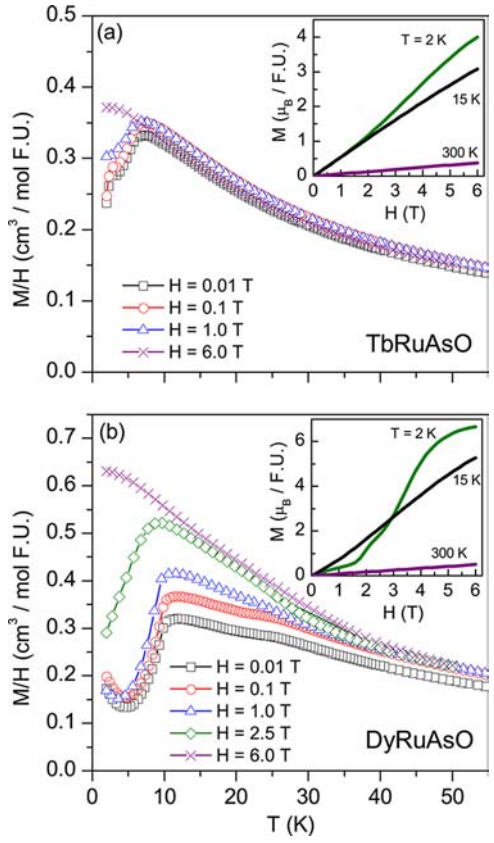

Figure 5. Results of DC magnetization measurements for (a) TbRuAsO and (b) DyRuAsO. The temperature dependence of the magnetic susceptibility (M/H) at the indicated applied magnetic fields (H) is shown in the main panels. The field dependence of the magnetic moment (M) at selected temperatures is shown in the insets.

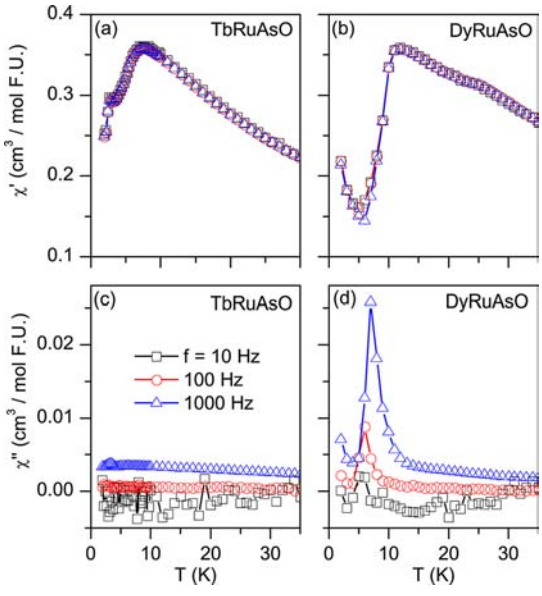

Figure 6. Real part (χ') and imaginary part (χ'') of the AC magnetic susceptibility of TbRuAsO (a and c) and DyRuAsO (b and d). Measurements were performed at the frequencies indicated in panel (c) and in zero applied DC field.

phase transition temperature T_S = 25 K. The response of the magnetic susceptibility at this temperature suggests that the transition at T_S may involve some incomplete or short-ranged

dx.doi.org/10.1021/ic3010695 | Inorg. Chem. 2012, 51, 8502−8508

ordering of Dy magnetic moments or a change in the magnetic moment of Dy because of modification of the crystalline electric field. Alternatively this may be a signature of magnetic ordering of small moments on Ru. Data for TbRuAsO also show a sharp anomaly near 2.5 K, which may indicate a second phase transition in this material, or may be a contribution from the impurity phase of cubic Tb_2O_3 identified in the powder diffraction analysis (Figure 1), which has an antiferromagnetic phase transition near this temperature.[38]

The imaginary part of the AC susceptibility (χ'') shown in Figure 6c for TbRuAsO and Figure 6d for DyRuAsO behave quite differently near T_N. This suggests that the antiferromagnetic transitions in TbRuAsO and DyRuAsO are fundamentally different. In particular, χ'' for DyRuAsO shows a peak below T_N which varies with frequency in both magnitude and position, indicating some dissipative component of the magnetic response. Although the orign of this behavior is unclear, it is likely related to the structural transition that occurs above T_N in DyRuAsO but not in TbRuAsO, and correlates with differences in behavior of other properties near T_N noted below.

The temperature dependence of the heat capacity (c_P) is summarized in Figure 7. Above about 50 K, c_P for the two

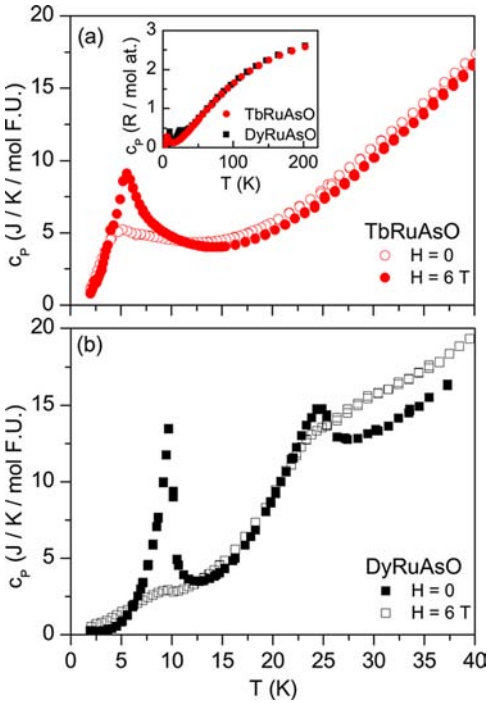

Figure 7. Results of heat capacity (c_P) measurements in zero applied magnetic field (closed symbols) and at H = 6 T (open symbols) for DyRuAsO (a) and TbRuAsO (b). The main panels emphasize low temperature phase transitions. The inset in (a) shows c_P in units of R for both materials up to 200 K.

materials is quite similar. In the absence of an applied magnetic field, sharp anomalies are observed near T_N in both materials. The small feature near 2.5 K in TbRuAsO corresponds to the lower temperature magnetic transitions noted in Figures 5 and 6, and may be due to the presence of cubic Tb_2O_3. In addition, a well-defined but broader peak occurs near T_S in DyRuAsO.

Application of a magnetic field affects all of the heat capacity anomalies. In DyRuAsO, the peak at T_N in nearly completely suppressed. This is typical for ordering transitions involving large magnetic moments, which interact strongly with an external field. The c_P anomaly at T_S in DyRuAsO responds to the magnetic field in a more unusual way, by broadening toward higher temperatures. If this is related only to the crystallographic transition, this behavior implies a strong coupling between the magnetism and the structural distortion. Alternatively, this observation may indicate some magnetic ordering occurs at T_S as well, and the c_P peak contains contributions from both the lattice and magnetism. If magnetic ordering does occur at T_S, it may involve small moments on Ru, since it occurs at a temperature higher than T_N and is not suppressed by the application of magnetic fields. The anomaly at T_N in TbRuAsO is diminished somewhat by the field, but is clearly still visible and significant at 6 T. This suggests that this transition involves more than simply the ordering of Tb moments, and may have a structural component or a contribution from Ru magnetism.

The magnetic ordering temperature is generally expected to increase across the early lanthanide series, reach a maximum at Gd, and decrease sharply from Gd to Tb to Dy and beyond, following the de Gennes factor $(g_J - 1)^2 J(J + 1)$ where g_J is the Landé g-factor and J is the total angular momentum.[39] In LnRuAsO, T_N is found to be <2, 4.5, 5.0, 7.0, and 10.5 K for Ln = Nd, Sm, Gd, Tb, and Dy, respectively.[34] The presence of transition metal magnetic ordering has been shown to have a strong effect on the lanthanide magnetic moments in similar materials.[40−45] The enhanced transition temperatures and magnetic field response of the heat capacity anomalies noted above may be indirect evidence of Ru magnetism in the Tb and Dy materials.

Figure 8 shows the results of transport property measurements. The resistivity (ρ) is moderately low and increases with temperature over the entire range investigated (Figure 8a), showing both materials to be metallic. The measured resistivity values for TbRuAsO and DyRuAsO are similar, and lower than those measured for the compounds with lighter lanthanides.[34] Quantitative comparisons of transport properties are complicated by the polycrystalline nature of the samples. With no applied magnetic field, the resistivity decreases upon cooling through T_N. This is attributed to the decrease in magnetic scattering of charge carriers in the ordered state. Application of a field of 6 T fully suppresses this feature in DyRuAsO, while only partial suppression is observed in TbRuAsO. This is similar to the behavior of the heat capacity anomalies at T_N. The resistivity does not show a response at T_S in DyRuAsO. The magnetoresistance of DyRuAsO is unusual, and seems to mimic the M vs H behavior shown in Figure 5b. Consistent with the metallic behavior, the Seebeck coefficient is small and positive for both materials at room temperature (~4 μV/K for TbRuAsO and ~2 μV/K for DyRuAsO), and decreases upon cooling.

Thermal conductivity (κ) measurements were performed to determine how the phase transitions affect heat transport. The results are shown in Figure 8b, which shows the low temperature behavior of the lattice thermal conductivity (κ_L), determined by subtracting the electronic contribution (κ_e) using the Wiedemann−Franz law ($\kappa_e = L_0 T/\rho$, $L_0 = 2.44 \times 10^{-8} W\Omega K^{-2}$). No anomalies are observed at T_N in TbRuAsO, or at T_S in DyRuAsO. However, a sharp feature is seen at T_N in DyRuAsO. This is somewhat surprising since no similar feature is seen in TbRuAsO, and indicates an important difference exists between the phase transitions at T_N or the ordered state below T_N in these two materials. The difference could arise from the fact that the antiferromagnetic ordering at T_N occurs

dx.doi.org/10.1021/ic3010695 | Inorg. Chem. 2012, 51, 8502−8508

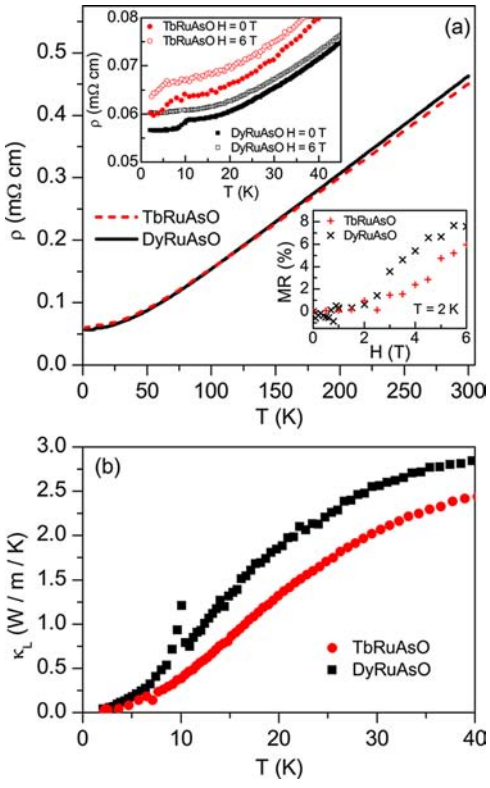

Figure 8. Transport properties of DyRuAsO and TbRuAsO. Electrical resistivity is shown in (a). The upper inset in (a) displays the low temperatures behaviors near the phase transitions, and the effects of applied magnetic fields on the temperature dependence. The lower inset shows the magnetoresistance (MR = $[\rho(H) - \rho(0)]/\rho(0)$) for each material measured at 2 K. Thermal conductivity data collected in zero magnetic field are shown in (b).

in the tetragonal structure of TbRuAsO, but the orthorhombic state of DyRuAsO. The strong response of κ_L at T_N in DyRuAsO is quite unusual. It suggests either strong interactions between heat carrying phonons and magnetic fluctuations above T_N, or that some other strong magnetoelastic interactions exist in this material. The existence of interactions between magnetism and phonons is supported by the observation of unusual behavior in both the thermal conductivity and the AC magnetic susceptibility at this temperature. Alternatively, this behavior could indicate that the transition at T_N is not simply a magnetic transition, but may have a structural component that could more directly affect the lattice vibrations.

These results show contrasting behavior between ZrCuSiAs-type ruthenium oxyarsenides containing neighboring lanthanides, and indicate strong coupling between crystal structure and magnetism. Further measurements, including neutron diffraction, are planned to directly probe the effect of magnetic field on the structural transition at T_S, and how the crystal structure responds to the magnetic transitions at T_N.

SUMMARY AND CONCLUSIONS

In summary, the structural and physical properties of the layered oxyarsenides TbRuAsO and DyRuAsO are reported at and below room temperature. Powder X-ray diffraction measurements show TbRuAsO to adopt the ZrCuSiAs structure-type (*P*4/*nmm*) over the entire temperature range investigated (15−300 K). This same structure is adopted by DyRuAsO at room temperature; however, a crystallographic phase transition is identified in DyRuAsO at T_S = 25 K. At this temperature, the structure distorts in the *ab*-plane, in a manner similar to certain compositions of $Fe_{1-x}Se$, but unique among ZrCuSiAs-type oxyarsenides. This results in an orthorhombic (*Pmmn*) structure at low temperatures. Anomalies in the magnetic properties are observed at this temperature as well, which may indicate that the structural distortion is accompanied (or driven) by short-ranged or partial magnetic ordering of Dy moments, a change in the magnetic ground state of Dy, or ordering of small magnetic moments on Ru. The absence of this structural distortion in TbRuAsO in the investigated temperature range suggests either suppression of possible Ru magnetism because of increased Ru−Ru distances, or significant differences in the lanthanide magnetic ground state energy of TbRuAsO and DyRuAsO in the distorted environment. Both materials undergo magnetic phase transitions, identified as long-ranged antiferromagnetic ordering of lanthanide magnetic moments, at T_N = 7.0 and 10.5 K for TbRuAsO and DyRuAsO, respectively. These values are higher than that reported for the Gd analogue. This observation, along with the relatively weak response to magnetic fields of the heat capacity anomalies at T_N in TbRuAsO and T_S in DyRuAsO suggest ordered magnetic moments on Ru may exist at low temperatures. Magnetic field induced phase transitions or moment reorientations were observed in the magnetically ordered state, particularly in DyRuAsO. In this material, strong magneto-elastic interaction are indicated by the experimental results. Indications include: (1) response to applied magnetic field of the heat capacity anomaly associated with the structural phase transition, (2) a sharp peak in the lattice thermal conductivity at T_N, (3) qualitatively different behavior in AC magnetic susceptibility, heat capacity, and thermal conductivity of orthorhombic DyRuAsO and tetragonal TbRuAsO at T_N. As expected, the room temperature structural properties follow established trends in the *Ln*RuAsO series. The present findings, however, highlight the important role that the identity of the lanthanide element can play on the physical properties of these materials in which structural, electronic, and magnetic properties are so intimately linked.

EXPERIMENTAL SECTION

Synthesis. Starting materials used for synthesizing polycrystalline samples of TbRuAsO and DyRuAsO were RuAs, Tb or Dy filings, and powders of $Tb_{11}O_{20}$ or Dy_2O_3. RuAs was made from reduced Ru powder (99.9%) and As pieces (99.9999%) by heating slowly to 1000 °C. Tb and Dy were filed from ingots (99.9%) in a helium glovebox. $Tb_{11}O_{20}$ was made by heating as received Tb_4O_7 (99.9%) in flowing oxygen at 450 °C. As received Dy_2O_3 (99.99%) was dried in air at 800 °C. Stoichiometric mixtures of these starting materials were thoroughly mixed by grinding in a helium glovebox, pressed into pellets in air, placed into capped alumina crucibles, and quickly transferred to a vacuum line for sealing in silica tubes which were evacuated and backfilled with about 1/5 atm of ultrahigh purity argon. Pellets were heated quickly to 1200 °C for 24−48 h. Subsequent firings at 1000−1200 °C were performed to improve sample purity.

Characterization and Properties Measurements. X-ray powder diffraction measurements were performed with a PANalytical X'Pert diffractometer and position sensitive detector using monochromated Cu $K\alpha_1$ radiation. Low temperature data collection employed an Oxford Phenix closed cycle cryostat. A Quantum Design Physical Property Measurement System was used for transport, heat capacity, and AC magnetic susceptibility measurements. A Quantum Design Magnetic Property Measurement System was used for DC magnetization measurements.

dx.doi.org/10.1021/ic3010695 | *Inorg. Chem.* 2012, 51, 8502−8508

■ ASSOCIATED CONTENT

Supporting Information

Crystallographic information (cif files) for TbRuAsO at room temperature and DyRuAsO at room temperature and 12 K. This material is available free of charge via the Internet at http://pubs.acs.org.

■ AUTHOR INFORMATION

Corresponding Author

*E-mail: McGuireMA@ornl.gov.

Notes

The authors declare no competing financial interest.

■ ACKNOWLEDGMENTS

Research supported the U.S. Department of Energy, Office of Basic Energy Sciences, Materials Sciences and Engineering Division.

■ REFERENCES

(1) Kamihara, Y.; Watanabe, T.; Hirano, M.; Hosono, H. *J. Am. Chem. Soc.* **2008**, *130*, 3296.
(2) Paglione, J.; Greene, R. L. *Nat. Phys.* **2010**, *6*, 645.
(3) Johnston, D. C. *Adv. Phys.* **2010**, *59*, 803.
(4) Johrendt, D.; Hosono, H.; Hoffmann, R.-D.; Pöttgen, R. *Z. Kristallogr.* **2011**, *226*, 435.
(5) Sefat, A. S.; Singh, D. J. *MRS Bull.* **2011**, *36*, 614.
(6) Mandrus, D.; Sefat, A. S.; McGuire, M. A.; Sales, B. C. *Chem. Mater.* **2010**, *22*, 715.
(7) Quebe, P.; Terbüe, L. J.; Jeitschko, W. *J. Alloys Compd.* **2000**, *302*, 70.
(8) de la Cruz, C.; Huang, Q.; Lynn, J. W.; Li, J.; Ratcliff, W., II; Zarestky, J. L.; Mook, H. A.; Chen, G. F.; Luo, J. L.; Wang, N. L.; Dai, P. *Nature* **2008**, *453*, 899.
(9) Nomura, T.; Kim, S. W.; Kamihara, Y.; Hirano, M.; Sushko, P. V.; Kato, K.; Takata, M.; Shluger, A. L.; Hosono, H. *Supercond. Sci. Technol.* **2008**, *21*, 125028.
(10) McGuire, M. A.; et al. *Phys. Rev. B* **2008**, *78*, 094517.
(11) Han, F.; Zhu, X.; Mu, G.; Cheng, P.; Wen, H.-H. *Phys. Rev. B* **2008**, *78*, 180503.
(12) Han, F.; Zhu, X.; Mu, G.; Cheng, P.; Wen, H.-H. *J. Phys. Soc. Jpn.* **2008**, *77*, 113709.
(13) Rotter, M.; Tegel, M.; Johrendt, D.; Schellenberg, I.; Hermes, W.; Pöttgen, R. *Phys. Rev. B* **2008**, *78*, 020503.
(14) Rotter, M.; Tegel, M.; Johrendt, D. *Phys. Rev. Lett.* **2008**, *101*, 107006.
(15) Kreyssig, A.; et al. *Phys. Rev. B* **2008**, *78*, 184517.
(16) Margadonna, S.; Takabayashi, Y.; McDonald, M. T.; Kasperkiewicz, K.; Mizuguchi, Y.; Takano, Y.; Fitch, A. N.; Suard, E.; Prassides, K. *Chem. Commun.* **2008**, 5607.
(17) Li, S.; de la Cruz, C.; Huang, Q.; Chen, Y.; Lynn, J. W.; Hu, J.; Huang, Y.-L.; Hsu, F.-C.; Yeh, K.-W.; Wu, M.-K.; Dai, P. *Phys. Rev. B* **2009**, *79*, 054503.
(18) Bao, W.; Qiu, Y.; Huang, Q.; Green, M. A.; Zajdel, P.; Fitzsimmons, M. R.; Zhernenkov, M.; Chang, S.; Fang, M.; Qian, B.; Vehstedt, E. K.; Yang, J.; Pham, H. M.; Z. Q. Mao, L. S. *Phys. Rev. Lett.* **2009**, *102*, 247001.
(19) Häggström, L.; Verma, H. R.; Bjarman, S.; Wäppling, R.; Berger, R. *J. Solid State Chem.* **1986**, *63*, 401.
(20) Sabrowsky, H.; Rosenber, M.; Welz, D.; Deppe, P.; Schäfer, W. *J. Magn. Magn. Mater.* **1986**, *54*, 1497.
(21) Ye, F.; Bao, W.; Wang, X. F.; Ying, J. J.; Chen, X. H.; Wang, H. D.; Dong, C. H.; Fang, M. *Phys. Rev. Lett.* **2011**, *107*, 137003.
(22) Guo, J.; Jin, S.; Wang, G.; Wang, S.; Zhu, K.; Zhou, T.; He, M.; Chen, X. *Phys. Rev. B* **2010**, *82*, 180520.
(23) Mozharivskyj, Y.; Kaczorowski, D.; Franzen, H. *Z. Anorg. Allg. Chem.* **2001**, *627*, 2163.
(24) Mozharivskyj, Y.; Pecharsky, A. O.; Bud'ko, S.; Franzen, H. *Z. Anorg. Allg. Chem.* **2002**, *628*, 1619.
(25) Christianson, A. D.; Lumsden, M. D.; Nagler, S. E.; MacDougall, G. J.; McGuire, M. A.; Sefat, A. S.; Jin, R.; Sales, B. C.; Mandrus, D. *Phys. Rev. Lett.* **2009**, *103*, 087002.
(26) Nandi, S.; Kim, M. G.; Kreyssig, A.; Fernandes, R. M.; Pratt, D. K.; Thaler, A.; Ni, N.; Budko, S. L.; Canfield, P. C.; Schmalian, J.; McQueeney, R. J.; Goldman, A. I. *Phys. Rev. Lett.* **2010**, *104*, 057006.
(27) Sefat, A. S.; McGuire, M. A.; Jin, R.; Sales, B. C.; Mandrus, D.; Ronning, F.; Bauer, E. D.; Mozharivskyj, Y. *Phys. Rev. B* **2009**, *79*, 094508.
(28) Zinth, V.; Petricek, V.; Dusek, M.; Johrendt, D. *Phys. Rev. B* **2012**, *85*, 014109.
(29) Sharma, S.; Bharathi, A.; Chandra, S.; Raghavendra Reddy, V.; Paulraj, S.; Satya, A. T.; Sastry, V. S.; Gupta, A.; Sundar, C. S. *Phys. Rev. B* **2010**, *81*, 174512.
(30) Schnelle, W.; Leithe-Jasper, A.; Gumeniuk, R.; Burkhardt, U.; Kasinathan, D.; Rosner, H. *Phys. Rev. B* **2009**, *79*, 214516.
(31) McGuire, M. A.; Singh, D. J.; Sefat, A. S.; Sales, B. C.; Mandrus, D. *J. Solid State Chem.* **2009**, *182*, 2326.
(32) Pallecchi, I.; Bernardini, F.; Tropeano, M.; Palenzona, A.; Martinelli, A.; Ferdeghini, C.; Vignolo, M.; Massidda, S.; Putti, M. *Phys. Rev. B* **2011**, *84*, 134524.
(33) Tropeano, M.; Cimberle, M. R.; Ferdeghini, C.; Lamura, G.; Martinelli, A.; Palenzona, A.; Pallecchi, I.; Sala, A.; Sheikin, I.; Bernardini, F.; Monni, M.; Sassidda, S.; Putti, M. *Phys. Rev. B* **2010**, *81*, 184504.
(34) McGuire, M. A.; May, A. F.; Sales, B. C. *J. Solid State Chem.* **2012**, *191*, 71.
(35) Ozawa, T. C.; Kauzlarich, S. M. *Sci. Technol. Adv. Mater.* **2008**, *9*, 033003.
(36) Pottgen, R.; Johrendt, D. *Z. Naturforsch.* **2008**, *63B*, 1135.
(37) Nitsche, F.; Jesche, A.; Hieckmann, E.; Doert, T.; Ruck, M. *Phys. Rev. B* **2010**, *82*, 134514.
(38) MacChesney, J. B.; Williams, H. J.; Sherwood, R. C.; Potter, J. F. *J. Chem. Phys.* **1966**, *44*, 596.
(39) O'Handley, R. C. *Modern Magnetic Materials: Principles and Applications*, 1st ed.; John Wiley and Sons, Inc.: New York, 2000.
(40) Marcinkova, A.; Hansen, T. C.; Curfs, C.; Margadonna, S.; Bos, J.-W. G. *Phys. Rev. B* **2010**, *82*, 174438.
(41) Emery, N.; Wildman, E. J.; Skakle, J. M. S.; Mclaughlin, A. C.; Smith, R. I.; Fitch, A. N. *Phys. Rev. B* **2011**, *83*, 144429.
(42) McGuire, M. A.; Gout, D. J.; Garlea, V. O.; Sefat, A. S.; Sales, B. C.; Mandrus, D. *Phys. Rev. B* **2010**, *81*, 104405.
(43) Marcinkova, A.; Grist, D. A. M.; Margiolaki, I.; Hansen, T. C.; Margodonna, S.; Bos, J.-W. G. *Phys. Rev. B* **2010**, *81*, 064511.
(44) Awana, V. P. S.; Nowik, I.; Pal, A.; Yamaura, K.; Takayama-Muromachi, E.; Felner, I. *Phys. Rev. B* **2010**, *81*, 212501.
(45) Skanthakumar, S.; Lynn, J. W.; Peng, J. L.; Li, Z. Y. *Phys. Rev. B* **1993**, *47*, 6173.